BBAA VI International Colloquium on:
Bluff Bodies Aerodynamics & Applications
Milano, Italy, July, 20-24 2008

AN INVESTIGATION OF THE AERODYNAMIC ADMITTANCES AND AERODYNAMIC WEIGHTING FUNCTIONS OF TRAINS

Mark Sterling[*], Chris J Baker[*], Abdessalem Bouferrouk[*], Hugh O'Neil[†], Stephen Wood[†], Wayne Pearce[††] and Ewan Crosbie[††]

[*]Department of Civil Engineering, School of Engineering
The University of Birmingham, Edgbaston, Birmingham, B15 2TT, UK
e-mail: m.sterling@bham.ac.uk

[†] Interfleet Technology Ltd, Interfleet House, Pride Parkway, Debry, DE24 8HX, UK
[††]RWDI Anemos Ltd., Unit 4, Lawrence Industrial Estate, Dunstable, Bedforshire, LU6 1BD, UK

Keywords: Aerodynamic admittance, Aerodynamic weighting functions, Trains.

ABSTRACT

Increasing train speeds combined with the predicted reduction in the weight of new trains ensures that the effect of crosswinds on train stability is of continued interest to the rail industry. Changes in the approaching wind velocity can in turn lead to changes in both the lift and side force on a vehicle. Calculations of the wind induced force can either be undertaken in the frequency domain with knowledge of aerodynamic admittance characteristics or in the time domain using aerodynamic weighting functions. This paper investigates the applicability of developing a universal aerodynamic admittance function and a corresponding analytical weighting function for a variety of train types based on a range of experimental data. It is suggested that only two variables are required to parameterise both the admittance and weighting functions. It is also argued that for certain train types one of these variables can be considered as a constant across a wide range of yaw angles.

1 INTRODUCTION

The stability of passenger trains and the dewirement of pantographs from overhead power cables are just two instances where the effect of cross winds can be of paramount importance. In order to examine either of these two problems in detail, a knowledge of the behaviour of the approaching wind and the induced response of the train is required. However, the complex nature of the wind in the lower part of the atmospheric boundary layer (ABL) and its interaction with the train can lead to the creation of addition flow structures which in turn can complicate the issue of predicting the wind induced forces. Nevertheless given sufficient information concerning the characteristics of the wind it is possible to begin to formulate a response to address these issues.

Conceptually, there are essentially two approaches which can be used to relate fluctuations in the wind to those on a vehicle. Such calculations are usually either performed in the frequency domain or the time domain. In the frequency domain it can be shown that:

$$S_{CFCF}(n) = 4C_F^2 \frac{S_{uu}(n)}{U^2} \left|X_F(n)\right|^2 \tag{1}$$

where $S_{CFCF}(n)$ is the power spectral density of the force coefficient, n is the frequency, C_F is the force coefficient, $S_{uu}(n)$ is the power spectral density of the streamwise component of the approaching wind, U is the mean velocity corresponding to the streamwise component of the wind and $|X_F(n)|^2$ is the aerodynamic admittance function. This approach embodies a number of fundamental assumptions regarding the behaviour of the flow around the train and the response of the train itself. These assumptions will be explored in detail in subsequent sections and their applicability to train aerodynamics will be examined.

In the time domain the quasi steady effects are usually incorporated through a convolution of the fluctuating streamwise velocity ($u'(t)$) and a weighting function $h_F(\tau)$:

$$f'(t) = \frac{1}{2} C_F \rho A \int_0^\infty h_F(\tau) u'^2(t-\tau) d\tau \tag{2}$$

where $f'(t)$ is the fluctuating force on the train and A is the side area. The relationships between the time and frequency domain can be expressed mathematically via Eqns. (3) and (4):

$$h_F(\tau) = \int_0^\infty \left|X_F(n)\right| e^{2\pi n i} dn \tag{3}$$

$$\left|X_F(n)\right| = \int_0^\infty h_F(\tau) e^{2\pi n i} d\tau \tag{4}$$

where i is the square root of minus one. This paper will examine a variety of experimental data in order to evaluate the aerodynamic weighting functions and aerodynamic admittances for a variety of train types. The data relating to the experimental work are outlined in section 2, while section 3 discusses the results of previous and current work in terms of the admittance function. Building on the work of the previous section, section 4 introduces a simple expression for the admittance function which is shown to fit a variety of train types for a variety of yaw angles. Finally, conclusions are presented in section 5.

2 THE MEASUREMENTS

Unfortunately there is only sparse data available in the public domain relating to this topic. Early model scale experiments undertaken in wind tunnels provided the main source of data prior to 2000. Three sources of data prior to 2000 will be investigated in this paper: Advanced Passenger Train (APT); a magnetically levitated vehicle (Mag-lev), [1]; and an idealised train (IT), [2]. All of the experiments were undertaken at model-scales of 1:50, 1:25 and 1:50 respectively. Further details relating to the simulations and the experimental data are available from [3].

In order to investigate the stability of the Class 390 "Pendolino" train in cross winds and to compare the data to that of a perceived "safe" vehicle (i.e. a Mark 3 coach), a series of full-scale experiments were undertaken at a coastal site at Eskmeals in Cumbria in the north west of England during the winters of 2001/02 and 2002/03, (see [4] and [5] for further details). Fig. 1 illustrates a schematic of the experimental geometry. The wind velocities was measured upstream trains using two ultrasonic anemometers (Model Gill R3-50, Biral) mounted at 3m and 10m above the ground. Additional anemometers were also mounted on a secondary mast in order to provide an insight into the profile of the approaching wind speed with respect to height above the ground. For the purposes of the current analysis, it is sufficient to report that data outlined below contained no unexpected behaviour, e.g. the data was stationary, and the turbulence intensity and surface roughness were consistent with this type of terrain [6].

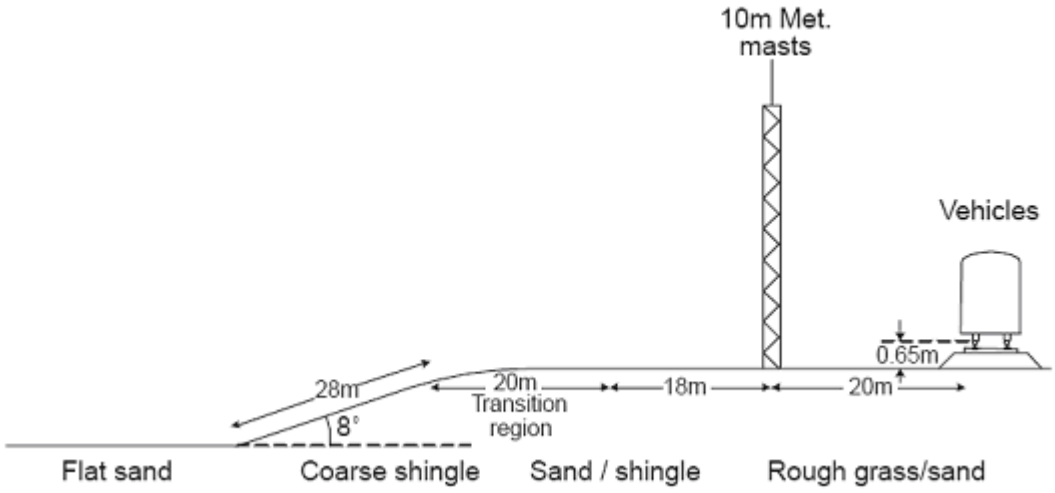

Fig. 1. A schematic of the site geometry for the full-scale experiments (source: [7]).

In the light of recent developments in the wind loading Codes of Practice in the UK, Europe and elsewhere, a perceived problem with respect to potential pantograph de-wirement between the pantograph arm and overhead cable arose. Hence, the Railway Safety and Standards Board (RSSB) funded a series of wind tunnel experiments on a $1/30^{th}$ model of a Class 365 EMU. The experiments were undertaken in an open return wind tunnel. Full details of the project can be found in [7] with an in depth analysis of the supporting data given in [8]. It is sufficient to note that the velocity profile matched the target ABL with a corresponding full-scale surface roughness of 0.03m. The turbulence intensity profile over a range corresponding to the vehicle height was appropriate [8] in addition to the corresponding velocity spectra [8]. An illustration of the wind tunnel experiments is given in Fig. 2.

Fig. 2. A schematic of the site geometry for the full-scale experiments (source: [4]).

3 EXPERIMENTAL RESULTS

3.1 Pre-2000 measurements

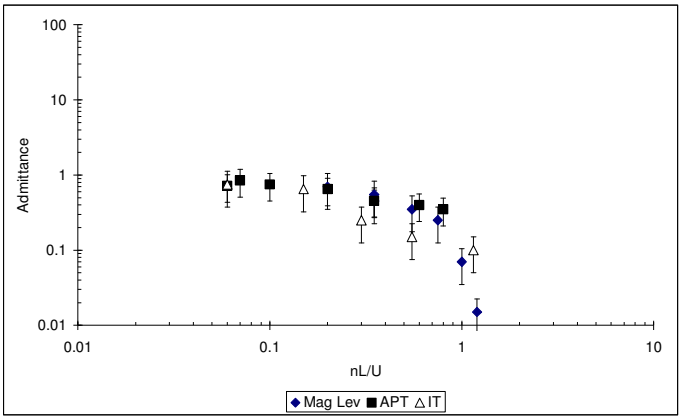

Fig. 2. Side force admittance data for the Mag-lev, APT and IT vehicles.

In what follows the data presented relate to the wind induced side forces only, and correspond to a limited set of yaw angles. These yaw angles are 76°, 90° and 90° for the Mag-lev, APT and IT respectively. Fig. 2 illustrates the aerodynamic admittance function for the Mag-Lev, APT and IT. The vertical axis in figure represents the admittance function as defined by Eqn. (1), while the horizontal axis represents the reduced frequency (actual frequency x length of a single vehicle / mean streamwise velocity). This format will be adopted throughout the paper. It should be noted that these data represent the mean values of admittance only and in all cases have a large degree of scatter, e.g. [9] states that the associated standard error (standard deviation/mean) is of the order of 38%. All of the data in Fig. 2 follow the same trend and indicate that as the reduced frequency tends to zero, the admittance tends towards unity, i.e. the large scale (low frequency) variations in the wind directly affect the forces measured on the trains. As the reduced frequency increases (turbulent scales reduce), the admittance rapidly decreases and takes into account the filtering that the inertia of the vehicle has on the flow, i.e. the lack of correlation of the gust structures.

3.2 Mark 3 coach full scale measurements

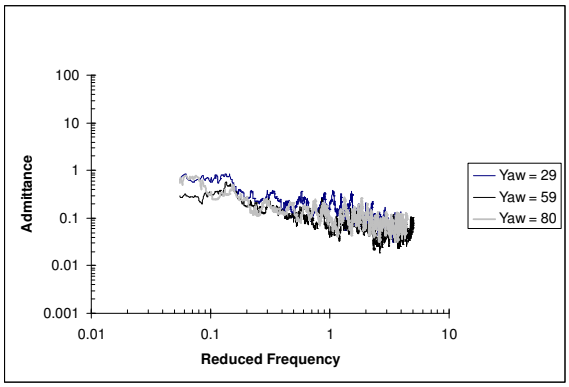

Fig. 3. Side force aerodynamic admittances for the Mark 3 coach

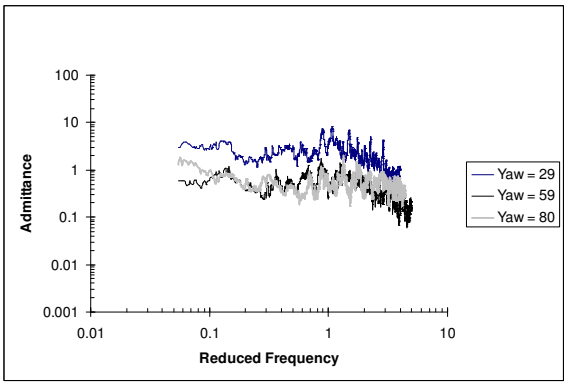

Fig. 4. Lift force aerodynamic admittances for the Mark 3 coach

Figs. 3 and 4 illustrates the side force and lift aerodynamic admittances respectively corresponding to the Mark 3 coach. Fig. 3 illustrates that the side force admittances all appear to collapse onto a single line, albeit with a significant amount of fluctuations. The lift force admittance data in Fig. 4 indicates similar trends to those outlined in Fig. 3, i.e. at low frequencies the admittances tends towards a constant value and decreases as the reduced frequency increases. Unlike the data in Fig. 3 the magnitude of the aerodynamic admittance appears to be dependant on yaw angle, e.g. the curve corresponding to a yaw angle of 29^o is displaced vertically upwards from the remaining yaw angles. The rate of change of the side force admittance with respect to reduced frequency appears to be greater than that of the corresponding lift force admittance. It is also noted that the lift force at a yaw angle of 29^o is greater than unity at low frequency.

3.3 Class 390 full-scale measurements

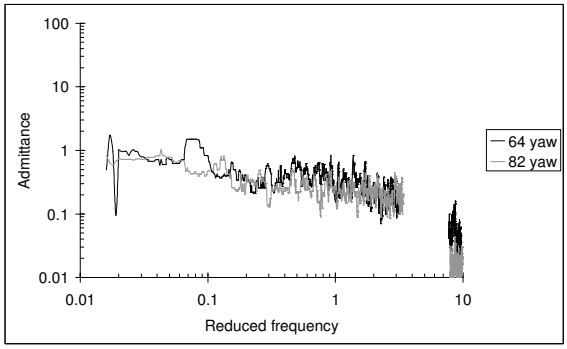

Fig. 5. Side force aerodynamic admittances for the Class 390

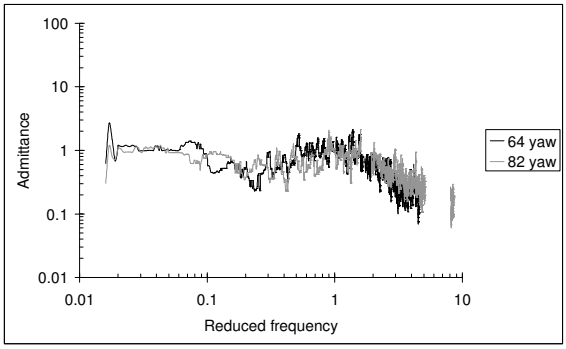

Fig. 6. Lift force aerodynamic admittances for the Class 390

Figs. 5 and 6 illustrate the aerodynamic admittance corresponding to the side and lift forces for the Class 390. In order to ease the interpretation of the aerodynamic effects, the effect of any vehicle suspension response has been removed, and is manifested by the gaps in the admittances. Such responses correspond to high frequency fluctuations and as such for the purposes of the current analysis it is considered not unreasonable to disregard this behaviour. The side force admittance data presented in Fig. 5 indicates that both sets of data appear to follow the same trend, a result which is consistent with the analysis of the Mark 3 data. The lift force data for the Class 390 (Fig. 6) also illustrates similar trends although the rate of decrease at high frequencies appears to be less than that of the side force. Although the data tends towards

unity at low frequencies there appears to be a peak in admittance at a reduced frequency of 0.1. This behaviour may arise as a result of vehicle induced turbulence.

3.4 Class 365 wind tunnel tests

The experiments for the Class 365 were undertaken in controlled conditions and as such data is available for a wide variety of yaw angles. These data are illustrated in Figs. 7 and 8. Fig. 7 illustrates that admittance varies with respect to yaw angle and at high yaw angles (>45^o) the admittance appear to collapse onto a single curve, albeit with a large degree of scatter. The same trend is apparent in the lift force (Fig. 8). It is also interesting to note that in the majority of cases as the reduced frequency decreases, the admittances tends towards values greater than unity. This issue will be addressed in the following sections.

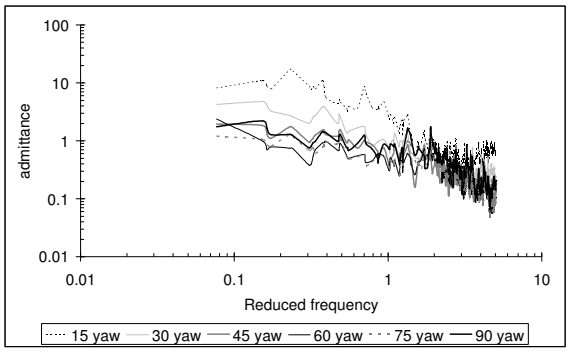

Fig. 7. Side force aerodynamic admittances for the Class 365

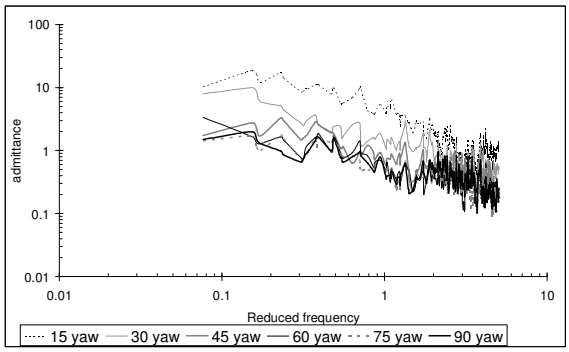

Fig. 8. Lift force aerodynamic admittances for the Class 365

4 FITTED AERODYNAMIC ADMITTANCES AND CORRESPONDING WEIGHTING FUNCTIONS

4.1 Initial comments concerning the aerodynamic admittances

In the previous section it was noted that a number of the admittance plots did not appear to tend towards unity at low values of reduced frequency. At first glance this is surprising since at low frequencies one would expect the fluctuations in the wind to follow the fluctuations in the longitudinal velocity. However, as outlined in section 1, there are a number of assumptions embodied within the aerodynamic admittance function, which it is perhaps worth revisiting. Firstly, the concept of an admittance function was initially developed in the 1960s for line-like structures, i.e. structures who do not significantly alter the flow around them and whose leading dimensions are significantly less than the longitudinal scale of turbulence. Both of these factors are not true for trains, since a train is essentially a bluff body and has characteristics dimensions similar to that longitudinal scale of turbulence. As a result both of these factors would result in low frequency admittances not tending towards unity. Secondly, body induced turbulence would add extra force fluctuations which again would alter the value of admittance at certain frequencies. However, perhaps the most influential factor for the current analysis concerns the height at which the streamwise velocity spectrum is measured. In

the above analysis this has been calculated at a full-scale equivalent height of 3m. While it is acknowledged that specifying a given height for such a calculation is important in terms of standardization, one must question the scientific implications of this approach. For example, this height might be where the stagnation streamline occurs, but need not necessarily be so. Indeed the concept of the stagnation streamline is far from robust for complex three dimensional bluff bodies at incidence to the flow.

Noting these above points it is postulated that it is not unreasonable to adjust all of the admittances by constant in order to ensure that they all tend towards unity at low values of reduced frequencies. While the scientific justification for this adjustment may be questionable, it is considered within the limits of the aforementioned assumptions and ensures that the form of all of the admittances can easily be compared. The affect of this adjustment is illustrated in Figs. 9-11 for all of the post 2000 data, and shows that all of data follow similar trends, albeit with a large amount of scatter. The legend has not been reproduced since it is only the form that is of interest.

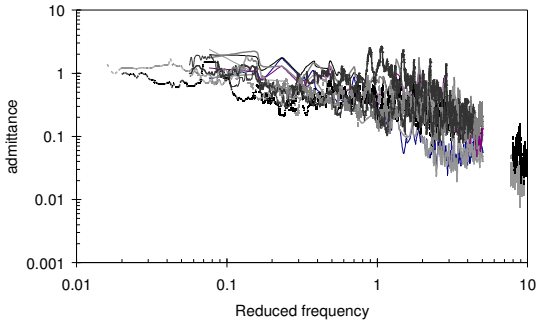

Fig. 9 Side force aerodynamic admittance (all post 2000 data)

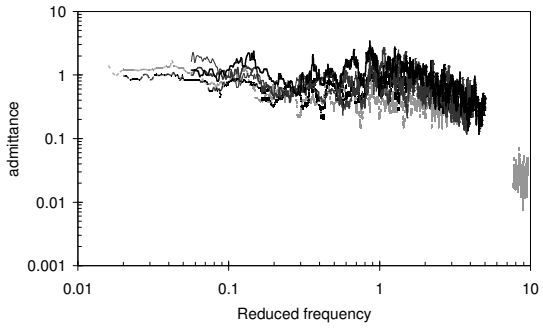

Fig. 10. Lift force admittance, all post 200 full-scale data

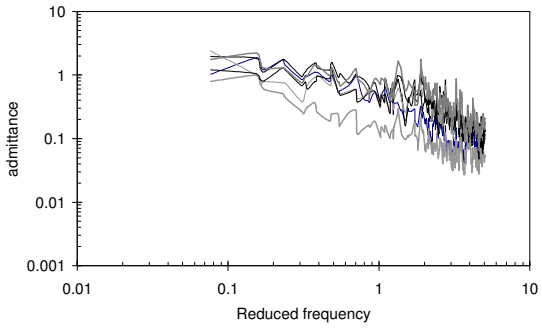

Fig. 11 lift force admittance, model scale data, Class 365

Examining the side force admittance data, there appeared to be no discernable trends between the different train types. Hence, all of this data has been presented as together in Fig. 9. However, examining the lift force data, the full-scale data and wind tunnel data appeared to show slight differences, namely a small reduced peak at a reduced frequency of less than unity in the full-scale data. This difference probably arises as a result of vortex induced phenomena over the roof of the train. For the purposes of the current analysis was decided to consider the full-scale lift force admittance separately from the corresponding Class 365 data.

4.2 General curve fitting

The previous subsection illustrated that providing the data has been adjusted correctly, the aerodynamic admittance functions appear to follow a similar trend regardless of yaw angle and / or train type. In order to simplify this further the following section will examine the possibility of fitting a simple curve to the admittance functions. The equation corresponding to the curve adopted is given in Eqn. (5):

$$\left|X_F(n)\right|^2 = \frac{1/k}{\left\{\left[1-\left(\frac{\bar{n}}{\bar{n}'}\right)^2\right]^2 + \left[2\xi\frac{\bar{n}}{\bar{n}'}\right]^2\right\}^{1/2}} \tag{5}$$

where $\bar{n}$ is the reduced frequency and *k,* ξ and $\bar{n}'$ are constants. The benefit of fitting an equation of the type shown in Eqn. (5) is that it that is has a corresponding an analytical form in the time domain, i.e.:

$$\bar{h}_F(\bar{\tau}) = a\sin(b\bar{\tau})\exp(-c\bar{\tau}) \quad \text{for} \quad \xi < 1.0 \tag{6a}$$

$$\bar{h}_F(\bar{\tau}) = d\bar{\tau}\exp(-c\bar{\tau}) \quad \text{for} \quad \xi = 1.0 \tag{6b}$$

$$\bar{h}_F(\bar{\tau}) = a'\sinh(b'\bar{\tau})\exp(-c\bar{\tau}) \quad \text{for} \quad \xi > 1.0 \tag{6c}$$

where $\bar{\tau} = \tau U / L$, $\bar{h}_F(\bar{\tau}) = h_F(\tau)L/U$, $a = \frac{2\pi\bar{n}'}{k\sqrt{1-\xi^2}}$, $a' = \frac{2\pi\bar{n}'}{k\sqrt{\xi^2-1}}$,

$b = 2\pi\bar{n}'\sqrt{1-\xi^2}$, $b' = 2\pi\bar{n}'\sqrt{\xi^2-1}$, $c = 2\pi\bar{n}'\xi$, $d = \left(2\pi\bar{n}'\right)^3 / k$ and L is a characteristic length.

In order to fit Eqn. (5) to the experimental data, the following assumptions were made:

- The value of *k* corresponding to each admittance function was considered to be given by the average value of the admittance for reduced frequencies of 0.1 and below.
- The parameters ξ and $\bar{n}'$ were varied and the corresponding values of admittance given by Eqn. (5) over the reduced frequency range were calculated.
- In order to evaluate the correct combination of ξ and $\bar{n}'$, the sum of the square of the difference between the measured data and that obtained from the fitted curve were evaluated for reduced frequencies greater than 1.0. The correct combination of ξ and $\bar{n}'$ was assumed to be given by the minimum value of this parameter. In what follows this parameter is termed the 'error'.
- ξ was varied over the range 0.1 to 10 in increments of 0.1.
- $\bar{n}'$ was varied over the range 1 to 11 in increments of 1.

Table 1 illustrates a set of various possible combinations for the parameters *k,* ξ and $\bar{n}'$. The value of k is relatively straight forward to specify. However, there are various combinations of ξ and $\bar{n}'$ which appear to give sensible results and the values in table 1 have been adopted in order to provide a common framework in which the data can be interpreted, i.e. in

a significant number of cases the value of $\overline{n}'$ can be seen to be 2.0. In some cases the best fit was obtained with different values of ξ and $\overline{n}'$ to those listed in table 1. In other words, there are a number of local minima in the 'ξ-$\overline{n}'$-error' surface. However, the maximum difference between the global minima on the 'ξ-$\overline{n}'$-error' surface and that corresponding to the local minima given by the value in table 1 was 17% for one set of data (Mark 3, 80° yaw, lift force). The maximum difference for the remaining data (excluding the pre 2000 measurements) was 3%. Given the variability in the experimental data these differences can be considered to be insignificant in terms of the current analysis.

Figs. 12 – 14 illustrates the appropriate fitted curves corresponding to the side force and lift force data presented in Figs. 9-11. In each case the value of $\overline{n}'$ was assumed to be 2.0, and the average value of ξ was obtained from the values in table 1 for the post 2000 data. Figs. 12-14 also illustrate the upper and lower bounds of the data using the results from table 1. Fig. 12 for all the side force data illustrates that at low and high frequencies the admittance envelope is relatively small. However, at a reduced frequency of 1.0 the difference in admittance between the upper and lower bound is ca. 0.78. This difference is not insignificant and again illustrates the variability in the data.

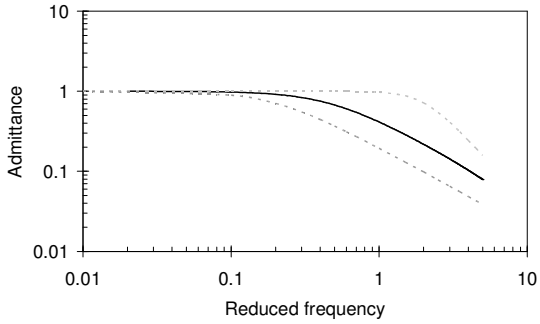

Fig. 12 Side force data (ξ = 2.3), upper bound (ξ = 0.7), lower bound (ξ = 5.1), & $\overline{n}'$ =2.0.

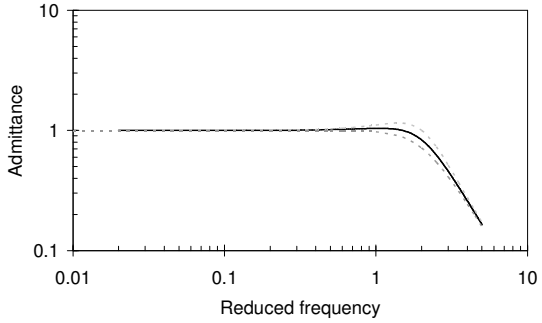

Fig. 13 Full-scale lift force data (ξ = 0.6), upper bound (ξ = 0.5), lower bound (ξ = 0.7), & $\overline{n}'$ =2.0

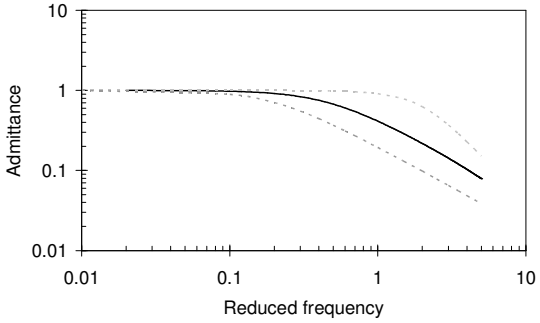

Fig. 14 Class 365 lift force data (ξ = 2.3), upper bound (ξ = 0.8), lower bound (ξ = 5.1), & $\overline{n}'$ =2.0

Fig. 13 illustrates the strong agreement between the full-scale lift force data, as evident by the relatively small size of the admittance envelope. For the case of the Class 365, the admittance envelope corresponding to the lift data has a similar form to that of side force. This is not too surprising given the range of ξ values adopted.

		Side force			Lift force		
Vehicle	Yaw (^{o})	k	ξ	$\overline{n}'$	k	ξ	$\overline{n}'$
Mag-Lev	76	1.0	10.4	1.0			
APT	90	1.3	3.1	1.0			
IT	90	1.3	3.0	2.0			
Mark 3	29	2.1	0.7	2.0	0.4	0.7	2.0
	59	3.5	2.4	2.0	1.8	0.5	2.0
	80	1.7	2.3	2.0	0.8	0.7	2.0
Class 390	64	1.0	1.6	2.0	0.9	0.7	2.0
	82	1.6	2.1	2.0	1.1	0.5	2.0
Class 365	15	0.1	4.9	2.0	0.1	2.5	2.0
	30	0.2	5.1	2.0	0.1	5.1	2.0
	45	0.5	3.0	2.0	0.6	3.0	2.0
	60	0.4	1.4	2.0	0.3	1.4	2.0
	75	0.8	1.2	2.0	0.7	1.2	2.0
	90	0.9	0.9	2.0	0.7	0.8	2.0

Table 1. Eqn. (5) parameters for the lift and side force aerodynamic admittances.

Using the results given in table 1 in conjunction with Eqn. (6) it is possible to obtain the aerodynamic weighting functions. The results of this procedure are illustrated in Figs. 15-17. The dotted lines in Figs. 15-17 correspond to the lower and upper bounds shown in Figs. 12-14. Both Figs. 15 and 17 illustrate almost identical features, i.e. a rapid increase in the value of the weighting function, followed by a gradual reduction. It is noticeable that the decrease in weighting function with respect to normalised time is significantly less for the "lower" bound data. In physical terms this suggests that the time history of the wind is significant in terms of the wind induced loading. As expected the "upper" bound data illustrates behaviour which is opposite to this, i.e. there is a large peak corresponding to a short time lag (ca. 0.1 normalised seconds). After this large peak the weighting function rapidly decreases and even attains a negative value. At this stage it is perhaps worth noting that the area under each of the normalised weighting curve functions tends to unity as the normalised time tends to infinity.

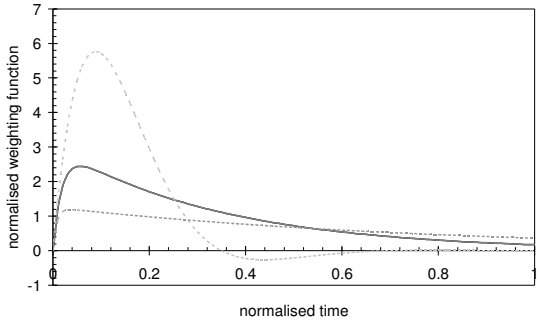

Fig15. Side weighting function

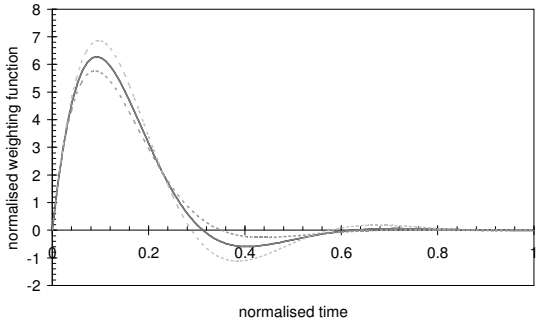

Fig. 16 Lift weighting function for the full-scale data

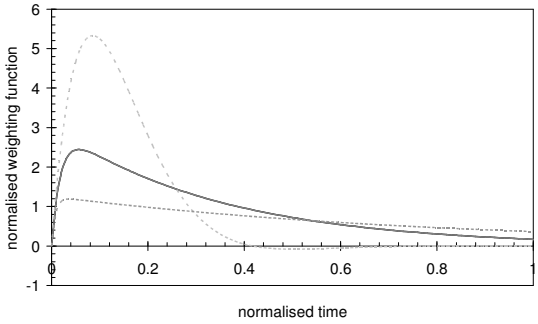

Fig. 17 Lift weighting function for the Class 365

5 CONCLUSIONS

This paper has examined a variety of datasets in order to explore both the behaviour of the aerodynamic admittances and the weighting functions with respect to train type and yaw angle. An attempt has been made to identify a universal function which can be used to represent both the side and lift aerodynamic admittance and one which can be represented analytically in the time domain. The following points can be made:

- All of the measured admittance functions follow the same general trend, i.e. at low frequencies they tend towards a constant value, whereas at high frequencies there is a rapid decrease.
- There is a wide range of variation in both the measured side force and lift force admittances. As such the data must be interpreted with care.
- It is possible to parameterise the mean characteristics of the aerodynamic admittances by an expression akin to that of a damped harmonic oscillator using three constants k, ξ, $\overline{n}'$.
- Surprisingly, the value of $\overline{n}'$ appears to be constant across a wide range of yaw angles for a variety of train types.
- With respect to the Class 365 data, there appears to be a general trend indicating a reduction in ξ as the yaw angle increases.
- Noting the large degree of variation in the data it is postulate that all of the data can be considered to collapse onto a single curve corresponding to the side force and a single curve corresponding to the lift force.

REFERENCES

[1] Howell, J and Everitt, K. W. (1983) Gust response of a high speed train model. In Aerodynamics of Transportation II (eds T. Morel & J Miller), 81-89. NEW York: ASME.

[2] Robinson, C. G. (1987) The effect of atmospheric turbulence on trains. PhD thesis, University of Nottingham.

[3] Baker, C J (1991) "Ground vehicles in high cross winds Part I,II&III: The interaction of aerodynamic forces and the vehicle system." Journal of Fluids and Structures, 5, 221-241.

[4] Baker, C.J., Jones, J., and Lopez-Calleja, F. (2003) Measurements of the cross wind forces on Mark 3and Class 390vehicles, Proceedings World Congress on Railway Research, Edinburgh.

[5] Ding, Y (2006). Unsteady crosswind forces on trains and corresponding aerodynamic parameters. PhD Thesis, The University of Birmingham.

[6] ESDU (1985), "Characteristics of atmospheric turbulence near the ground: Part 2 Single point data for strong wind - neutral atmosphere", data Item 85020, Engineering Sciences Data Unit, London.

[7] Bouferrouk, A., Sterling, M and Baker C J (2008) Calculation of the cross wind displacement of pantographs. BBAAVI, 6th International Colloquium on Bluff Bodies Aerodynamics and Applications. 27 – 31 July, Milan, Italy.

[8] Baker, C. J, Sterling, M and Bouferrouk, A. (2008) Aerodynamic forces on electrical multiple unit trains in cross winds. BBAAVI, 6th International Colloquium on Bluff Bodies Aerodynamics and Applications. 27 – 31 July, Milan, Italy.

[9] Cooper, R.K (1981) The effect of cross wind trains. AMSE Journal of fluids engineering, 1093, 170-178.